JOURNAL OF MATERIALS SCIENCE 8 (1973) 1383–1400

Superconductivity of heat-treated Nb-65 at.% Ti alloy

M. J. WITCOMB*, D. DEW-HUGHES,
Department of Physics, University of Lancaster, Lancaster, UK

Brief reviews are given of the effect of heat-treatment on the microstructure of cold-worked bcc metals and the superconducting properties of niobium alloys. Particular attention is paid to the influence of interstitial impurities in these processes. The annealing effects in microstructure and superconducting properties of a cold-worked Nb-65 at. % Ti alloy, containing oxygen as a major impurity, have been studied. The precipitation process takes the form βTiNb + $O_2 \rightarrow$ various Ti oxides $\rightarrow \alpha$Ti + TiO. Differences in precipitation sequence are described for vacuum-annealing and annealing in impure argon. Flux-pinning is related to the microstructural observations. At least three pinning mechanisms appear to operate; dislocation pinning and two types of precipitate pinning. These observations are in accord with previously proposed pinning models.

1. Introduction

The effect of microstructure upon superconducting properties has been reviewed elsewhere [1]. The quantity of major interest is the critical current density, J_c, whose value is determined by the strength of the interaction (pinning) between quantized flux vortices (flux lines) and microstructural features of the material (pinning centres) which cause a local variation in superconducting properties. This problem has been considered in previous articles in this journal for cold-worked niobium alloys [2] and for a deformed and annealed molybdenum-rhenium alloy [3].

A wide variety of microstructures may be produced by heat-treatment of deformed alloys. The effect of heat-treatment upon superconducting properties of many alloys has been reported; though in many cases the results are of little value owing to an imperfect understanding of the microstructural changes brought about by the heat-treatment. These include dislocation rearrangements, phase transformations and precipitation, all complicated by the presence of interstitial impurities. The latter are particularly important in alloys of bcc transition metals, which are capable of dissolving relatively large quantities of interstitials, and are indeed difficult to prepare without such contamination.

This paper reports the study of a niobium 65 at. % titanium alloy, containing oxygen. The alloy was chosen because it is close to the composition of commercial material currently used in the construction of superconducting solenoids, and because it was known that heat-treatment could strongly influence its superconducting properties. The microstructural changes consequent upon annealing were determined in detail using transmission electron microscopy, and compared with measurements of superconducting properties. The paper begins with two brief reviews, one of the microstructure of annealed bcc metals, and the other of previous work on the superconductivity of annealed niobium alloys.

2. Microstructure of annealed bcc metals

2.1. Deformed, interstitial-free metals

Studies of heat-treatment effects on microstructure of cold-worked bcc metals indicate that the mechanisms involved are probably the same as those for fcc materials, apart from crystallographic differences in slip systems. A similar conclusion has previously been reached

*Present address : Electron Microscope Unit, University of the Witwatersrand, Johannesburg, South Africa.

with regard to deformation microstructures in these materials [2].

In the absence of interstitial impurities, heat-treatment produces a vacancy-controlled, cold-work dependent, recovery/recrystallization process. In the deformed bcc metals such as α-Fe [4-6], Mo [6, 7], Nb [8, 9], Ta [10, 11], V [9], W [12, 13] , dislocations are partially arranged in cell structures or in sub-boundaries, giving diffuse cell structures. The recovery process causes the cells to sharpen and the sub-boundaries to grow slightly. In materials having uniformly distributed dislocations after deformation, in particular α-Fe deformed at low temperatures [5, 6], and deformed Nb-Ta [2, 9], Nb-V [14] alloys, recovery involves formation, sharpening and growth of sub-boundaries. The stacking fault energy of the metal strongly influences the occurrence and definition of the cell structure [15-17].

At later annealing stages, the majority of dislocations are annihilated; some of those remaining rearrange by a climb process into small-angle polygonization or sub-grain boundaries. The factors influencing subsequent recrystallization are [18]: (i) amount of prior deformation and deformation temperature, (ii) annealing temperature, (iii) grain size prior to plastic deformation, (iv) specimen purity. The localized disorientations in the deformation dislocation configuration serve as nucleation sites, hence new grains preferentially form at microband regions rather than at normal deformation bands [19].

2.2 Deformed metals containing interstitials

The kinetics of annealing processes may be dependent upon the rate of diffusion of the interstitials, rather than upon self-diffusion of the alloy. There are at least five possible reactions involving interstitial elements upon heat-treatment.

2.2.1. Dislocation pinning

Interaction between interstitial-dislocation stress fields lowers total strain energy. An attractive force thus induces interstitial atoms to segregate to the centre of the dislocations. If diffusion time is sufficient, a solute atom atmosphere forms round each dislocation [20] and produces a restraining or locking, Cottrell or Snoek, mechanism on dislocation movement. In contrast to fcc metals, interstitial solute atoms in bcc lattices produce large volume expansions and large tetragonal distortions. The latter are asymmetric, and can thus interact with both shear and hydrostatic stresses to lock screw and edge dislocations [21]. Relatively higher temperatures are then needed to break the dislocations away and cause dislocation rearrangement.

2.2.2. Pseudo-precipitates

Through the above stress effect, interstitials experience an attractive force towards dislocation cell walls. Since impurity distribution is unlikely to be uniform, and both dislocation density and configuration within cell walls will be irregular, the force on interstitials will vary from area to area, resulting in local variations in impurity concentration. Dislocations will be firmly locked either by solute atom segregation or, since local concentrations could considerably exceed the solubility limit, by fine precipitation of an impurity phase along their length such as seen in αFe-C [22], αFe-N [23], and Nb-N [24]. It should be noted, however, that in a heavily strained lattice the normal solubility may have little significance. Formation of ordered solid solutions containing many at. % of impurity in the cell walls may be possible [25]. In addition, since impurities lower the stacking fault energy of bcc metals and cause splitting of dislocations into partials [6], a greater accommodational area is produced for interstitials. By these interstitial migration effects, dislocation cell walls can be effectively transformed into pseudo-precipitates.

2.2.3. Domain ordering effects

A transformation from disorder, with interstitials in random positions, to an ordered state, with interstitials in specific lattice locations forming a superlattice structure, can occur on cooling heat-treated bcc metals. Both annealing and dissimilar atom attraction [26, 27] provide diffusion activation for this co-operative phenomenon. The transition, noted especially in Nb-O [28-31], Nb-Ta-O [9], Ta-C [32], Ta-H [33], and Ta-N [34], occurs by nucleation and growth, the latter proceeding in strict crystallographic directions, often appearing as a cross-hatched pattern [31]. The nucleation process can be either homogeneous or preferential [35, 36]. In the latter case edge dislocations, as a result of anisotropic stress fields, can produce domain growth in preferred orientations along their length [29].

2.2.4. Shear type precipitates

Rapid cooling from high temperature of some supersaturated bcc solid solutions containing interstitials can cause a shear transformation. It is generally diffusionless and generates a metastable martensite type phase [37]. The product has definite crystallographic habit and lattice orientation relationship with respect to the parent phase. The amount obtained depends on the final temperature, the transformation being accelerated by cold work. The martensite plates attain their shape by two successive shear displacements contained in boundaries coherent with the parent phase. The first is a homogeneous shear throughout the plate and occurs parallel to a specific parent phase habit plane. The second, a lesser displacement, takes place via slip or twinning.

2.2.5. Massive precipitates

In contrast to individual solute atoms or atmospheres, these are discrete second phase particles. The initial precipitate is not necessarily the same structure as the equilibrium phase since during annealing it can pass through intermediate non-stoichiometric structures of varying degrees of coherency with the matrix [38]. Impurity absorption from the annealing atmosphere can alter the precipitate composition with time as well as producing an interstitial, and hence precipitate composition, gradient through the specimen.

2.3. Two-phase alloys

The group IV A elements Ti, Zr and Hf are polymorphic, being hcp at low temperatures but bcc above several hundred °C. When alloyed with the group V A bcc metals V, Nb,Ta they form a continuous bcc solid solution at high temperatures, which in group IV A–rich alloys transforms to an hcp phase at low temperatures. Quenching of these alloys from the bcc region causes a diffusionless, martensitic transformation, the products of which by subsequent ageing pass through a series of metastable precipitates before reaching the equilibrium two-phase structure. This has been most thorougly investigated in Nb-Ti [39-42] and also observed in V-Ti [43, 44]. Nb-Zr [45], Nb-Hf [46] and V-Ti [47] also undergo a monotectoid reaction which produces two bcc phases of differing composition.

The presence of interstitials affects not only the kinetics of these phase transformations, but also the equilibrium compositions of the resulting phases, TTT and phase diagrams being considerably altered. The monotectoid in V-Ti [47] as well as that in Nb-Zr [48] is believed to occur only in the presence of impurities. The microstructure of annealed Nb-Zr alloys has been studied by Waldron [49]. The stabilization of normally non-equilibrium phases by the presence of interstitials is possible in all of these systems.

From this brief survey, the complexity of possible microstructural changes on annealing cold-worked alloys contaminated with interstitial impurities will be appreciated. Because interstitials affect the kinetics of dislocation rearrangement and phase transformations, it is quite unsafe to attempt to predict behaviour from that of uncontaminated alloys.

3. The effect of heat-treatment on superconductivity of Nb alloys

The major part of the work on alloy superconductors to date has been based on niobium, the principal alloying constituents being the transition elements Ta, Ti and Zr. These alloys, which may also contain significant amounts of the interstitial elements carbon, hydrogen, nitrogen and oxygen, have, as a general rule, been subject to some kind of deformation. Heat-treatment effects on such systems can become highly complex and the subsequent flux line interaction is difficult to analyse. Attention is focused on Nb-Ti alloys, since their commercial importance has generated much investigation; results are discussed only where a relatively clear interpretation can be given. All alloy compositions quoted are in at. %.

The effect of dislocations on superconducting properties is well documented [1, 2, 50-52]. Pinning by such defects is known to be in no way significantly different from that by second-phase particles [1]. Uniform dislocation distributions such as seen in Nb-50Ta [2] and Nb-V [14] cause little flux-trapping. Suitable heat-treatment can produce marked hysteresis effects by rearranging the dislocations into non-uniform arrays which are more effective flux barriers. The high magnetization and critical current values characteristic of three-dimensional dislocation cell and fibre structures can be increased by low-temperature annealing, at about 500°C, through increased dislocation density in, and sharper definition of, the cell walls. Such behaviour has been observed for Nb-40Ti [53], Nb-25Zr [54, 55] and has been

implied from critical current/activation energies for Nb-23, 55, 75, 79Ti [25, 26]. Annealing at higher temperatures decreases magnetic irreversibility through the reduction in all-over dislocation density and increase in cell diameter. Baker [57] and Neal *et al* [58] have shown for Nb-60Ti that the critical current is inversely proportional to cell or fibre diameter; the smaller the cell diameter, the more pinning points or cell walls per unit length of flux line. Dislocation rearrangements in the cell wall have been postulated for increased pinning in Nb-60Ti by Hampshire and Taylor [59]. Specimen hysteresis need not dramatically decrease with extensive recovery since polygonized and sub-grain structures can still cause strong flux line pinning, in some cases, greater than that from unrefined cell structures [53]. In heavily ($> 90\%$) cold worked strip specimens, such as rolled Nb-Hf [60], Nb-Sc [61, 62], Nb-Ti [63,64] and Nb-Zr [65, 66], dislocation structure and critical current are anisotropic. Heat-treatment causes the dislocation structure to become less uniform in the rolled surface while in the end-sections the cells behave as fibres in wires and coarsen [57]. Such behaviour increases critical current while reducing anisotropy.

Precipitate nucleation on cell walls, such as α-phase precipitates on dislocation fibre walls in Nb-67, 80Ti [67] and Nb-15Zr-45Ti [68], causes marked enhancement of critical current values. Maximum pseudo-precipitate characteristics for the wall occur when the precipitate distribution is uniform along its length [69]. Pfeiffer and Hillman [67] have shown further that for Nb-67, 80Ti additional deformation after heat-treatment removes recovery substructure and produces finer precipitates. An even finer cell structure can then form round the particles as nodes of the structure, as first suggested by Dew-Hughes [52]. Both effects lead to increased critical current.

Marked variation in flux-pinning as precipitate type, precipitate and matrix composition, are altered as a result of heat-treatment of martensite transformation products, has been demonstrated in Nb-80Ti [41, 70]. The importance of particle separation on critical current values has been demonstrated for ω-phase precipitates in Nb-78Ti [71].

The presence of interstitials in bcc alloys, as in bcc metals, will affect the kinetics of dislocation rearrangement during annealing while segregation to various defects will enhance their effectiveness as flux-pinning sites. Baker [57] has shown that temperatures needed to produce equivalent dislocation motion, rearrangement and critical current values in supersaturated solid solution Nb-60Ti alloys containing interstitials are 100°C higher than for the undoped material. The work of Charlesworth and Madsen [25, 56] and Penney *et al* [72] on heavily cold-worked Nb-Ti indicates that at low annealing temperatures up to about 300°C for Nb-20, 23Ti and 200°C for Nb-55Ti, the fall observed in critical current is due to recovery causing dislocation annihilation and a reduction in dislocation density. Annealing in a temperature range 200°C higher, however, causes interstitial migration to dislocations in the cell walls and an increase in critical current. The temperature-range differences between alloys is believed to be related to the dislocation cell dimensions [56]. As yet, all reports of interstitials in cell walls have been postulated from indirect measurements. The high dislocation densities in cell walls and associated contrast make interstitial observation difficult, if not impossible.

The effect of interstitials on phase transformations has already been mentioned. Increasing critical current with oxygen and carbon impurities in Nb-25Zr [73, 74] and Nb-50Ti [75] has been clearly demonstrated. Reuter *et al* [76] have shown for Nb-57Ti that simultaneous precipitation of different phases is possible. An extension of this work by Rauch *et al* [77] showed that the lower the oxygen interstitial level and hence different phase precipitated, the lower the optimum ageing temperature for critical current. Precipitates may also form by martensitic type reaction from supersaturated solid solution. Narlikar [9] has shown bcc Nb to transform to fcc NbO domain structures when cold worked niobium is air-annealed at 1500°C for 60 sec. Annealing Nb, Nb-Ta and Nb-Ti at 1200 to 1350°C in argon containing oxygen as an impurity [9] resulted in an ordered oxide domain structure similar to that reported by Gevers *et al* [78] and Landuyt *et al* [30]. Flux-pinning by these boundaries was equivalent to that from the cold-worked dislocation structure [9]. A factor of 10 increase in critical current has been reported for Nb-0.860 when 20% of the oxygen atoms form NbO domains [79].

4. Experimental techniques

The niobium 65 at. % titanium alloy was

supplied by the International Research and Development Co Ltd, Newcastle upon Tyne. It was in the form of thin strip about 0.2 mm thick, had been cold-worked $> 90\%$ and contained approximately 400 ppm of nitrogen and 3000 ppm oxygen. Thin foils, parallel to the plane of the sheet, were prepared for transmission electron microscope examination by chemical thinning at room temperature using a solution of 50% nitric, 30% sulphuric and 20% hydrofluoric acids. Annealed specimens required a different composition; with increasing annealing temperatures the solution tended to 70% HNO_3, 10% H_2SO_4, 20% HF. The foils were subsequently examined in a Siemens Elmiskop 1A electron microscope operating at 100 kV. Specimens were prepared for optical microscopy using the above polishing solution followed by a quick dip in hydrofluoric acid. Debye-Scherrer X-ray patterns were obtained by rotating a 1 mm strip of each heat-treated specimen in a 114.6 mm diameter powder camera.

Normal-state resistivity was measured using a four-contact method with the specimen at a temperature slightly in excess of T_c. Magnetization measurements were made on specimens 10 mm × 2 mm × 0.2 mm at 4.2K by an automatic method [80]. Critical current values were determined at 4.2K on specimens 70 mm long, 0.5 mm wide, and 0.2 mm thick, mounted in hairpin configuration and subjected to different applied transverse fields from a battery-energized Bitter solenoid at the Royal Radar Establishment, Malvern. The field could be varied only in steps of a few KOE, and accurate determination of H_{c2} was not possible. Current and potential connections were made to the specimen by clamping indium-coated capillary tube on to it.

5. Microstructure of Nb-65Ti

5.1. As-received material

Transmission electron microscopy of the as-received material revealed a fairly high dislocation densitied microstructure. The dislocation distribution was heterogeneous, some areas showed uniform distributions while others exhibited non-uniform arrangements, in particular, cell structures (Fig. 1). The average cell diameter is ~ 0.3 μm and cell wall thickness ~ 0.05 μm.

5.2. Vacuum-annealing

Annealing the as-received material at 300°C for 1 h in a vacuum of 1.33×10^{-2} Nm^{-2} caused nucleation of second phase particles approximately 30 nm in width (Fig. 2). Electron diffraction identified these as a hexagonal oxide phase δTiO_x where $x \approx 0.5$ [81]. Heat-treatment at 550°C for half an hour resulted in the growth of these precipitates into a platelet form having lenticular cross-section with a width of ~ 100 nm and a length of ~ 2 μm (Fig.

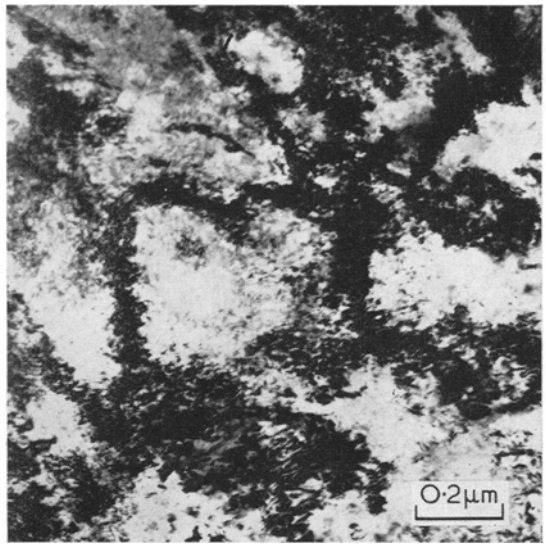

Figure 1 Dislocation cell structure of the cold worked Nb-Ti.

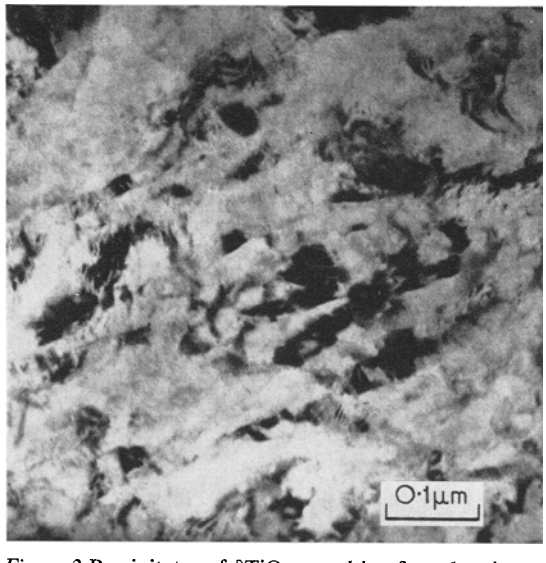

Figure 2 Precipitates of $\delta TiO_{0.5}$ resulting from heating at 300°C for 1 h at $133 \times 10^{-4} Nm^{-2}$.

3). Internal twinning of these particles was sometimes evident (Fig. 4). Diffraction studies revealed that although the precipitates obtained by this treatment indexed as δTiO_x, the c-parameter and, hence, oxygen content had increased slightly. Further annealing at this temperature resulted in more precipitate growth and much more internal precipitate twinning. Dislocation rearrangement after a 10 h heat-treatment replaced the cell structure by polygonized structures (Fig. 5) together with a few small recrystallized grains. Prolonged heating, 50 h, at 550°C produced (Fig. 6) the nucleation of a completely new phase, tetragonal αTi-TiO, alternatively known as δ [82]. No information concerning the homogeneity range of this

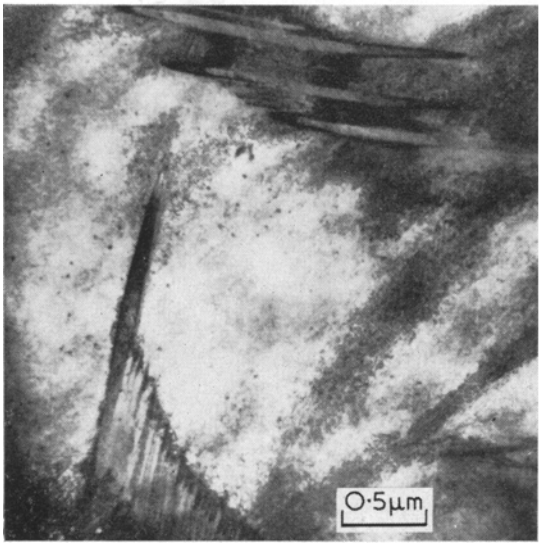

Figure 3 Lenticular shaped precipitates in ½ h at 550°C vacuum annealed Nb-Ti.

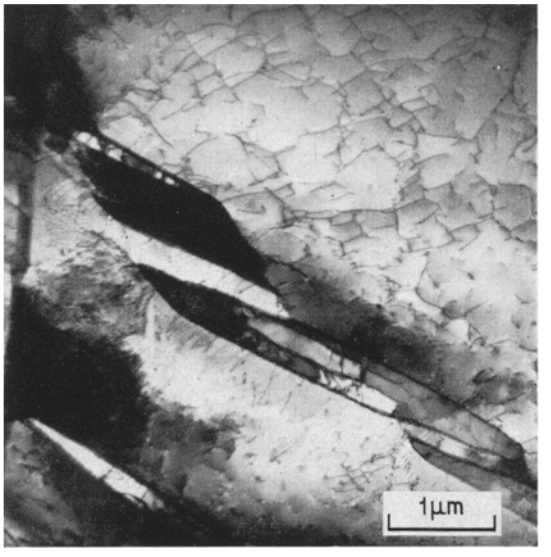

Figure 5 Precipitates and polygonized structures in 10 h at 550°C material.

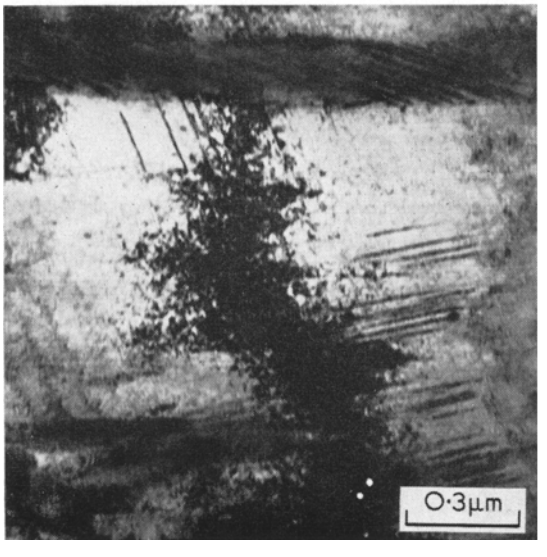

Figure 4 Evidence of precipitate twinning in material heated at 550°C for ½ h.

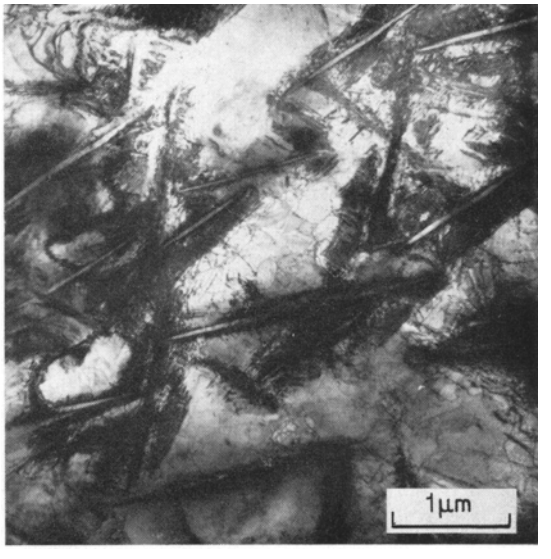

Figure 6 Precipitates of αTi-TiO after annealing Nb-Ti for 50 h at 550°C in vacuum.

phase is available, but it does occur in a composition range which includes Ti_3O_2 and Ti_4O_3 and is believed to be ~40 at. % oxygen [82]. These precipitates appear as plates with lengths 1 to 2 μm and a width of 40 nm, spaced from 0.2 to 1 μm.

5.3. Argon-annealing

In contrast to vacuum-annealing, heat-treatments performed in an argon atmosphere yielded a much more complex microstructure. This result is a direct consequence of oxygen impurity in the argon.

Annealing at 400°C for 1 h revealed the characteristic process of dislocation rearrangement toward a cell structure throughout the material. In addition, precipitates were also observed, (Fig. 7). Heat-treatment at 400°C for 2 h and at 450°C for 1 and 2 h showed similar precipitation effects although for the first and last treatments, a uniform distribution of very fine precipitates, ~20 nm × 50 nm in size, was also observed (Fig. 8). Material subject to 5 h at 450°C exhibited long, narrow, presumably lenticular precipitates of width ~10 nm and length ~100 nm, lying along preferred directions (Fig. 9).

Three distinct precipitate forms can be seen in the microstructure of material heated to 550°C for 1 h. One is large martensite-like twinned precipitates, ~1 μm in width, (Fig. 10); networks of dislocations are visible in and between these precipitates. Elsewhere, smaller parallel precipitates, ~20 nm × 500 nm (Fig. 11), and elliptical particles, ~100 nm × 150 nm (Fig. 12), were observed. The latter appear to

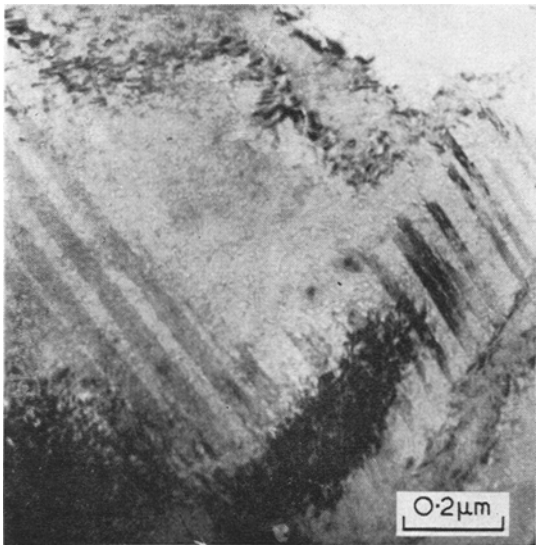

Figure 7 Evidence of precipitate nucleation on dislocation cell walls in argon annealed, 1 h at 400°C, Nb-Ti.

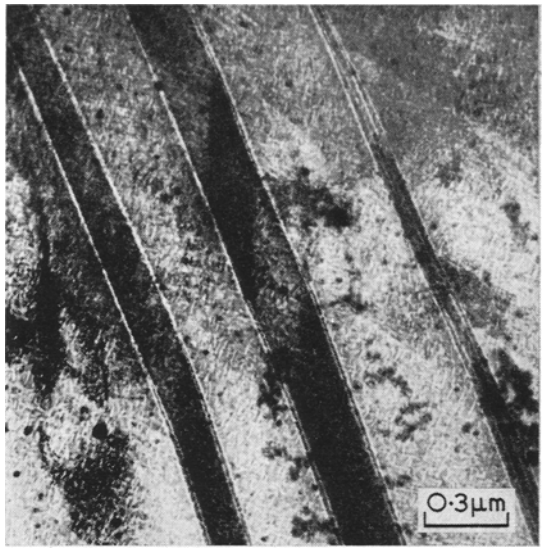

Figure 8 Both large and very fine precipitates in material heated 2 h at 400°C.

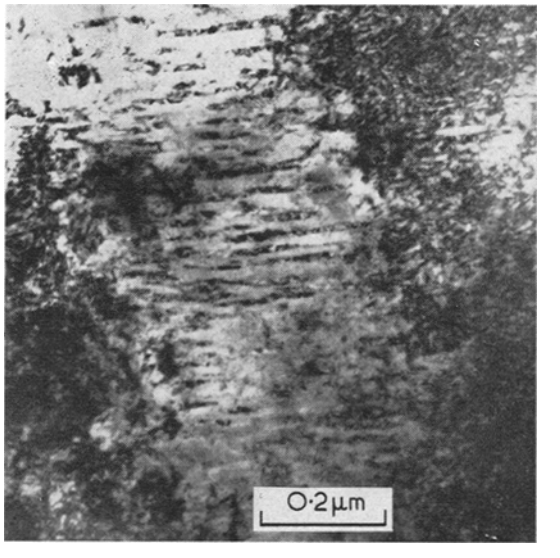

Figure 9 Long narrow precipitates in 5 h at 450°C argon heated Nb-Ti.

be small precipitates surrounded by rings of dislocation; their appearance is similar to that caused by the relief of coherency strains by dislocation rings around θ'' particles in Al-4% Cu [83]. Little change occurs in the microstructure on heating for 5 h at 550°C (Fig. 13). The fat platelets are believed identical to the small narrow precipitates also seen, but in a different orientation. These could well be the result of enlargement of the elliptical particles seen in material annealed for 1 h. Independent electron-diffraction patterns could not be obtained from these particles owing to specimen thickness. Moiré images as well as dislocation networks can be resolved on these precipitates. The former give credence to the idea of coherency strains

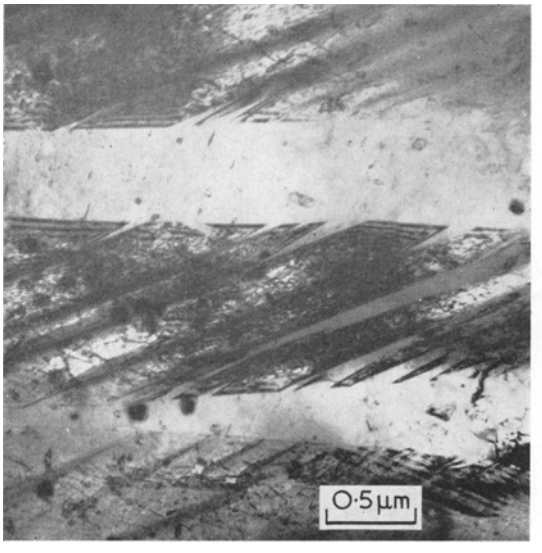

Figure 10 Large twinned martensitic type precipitates in 1 h at 550°C material.

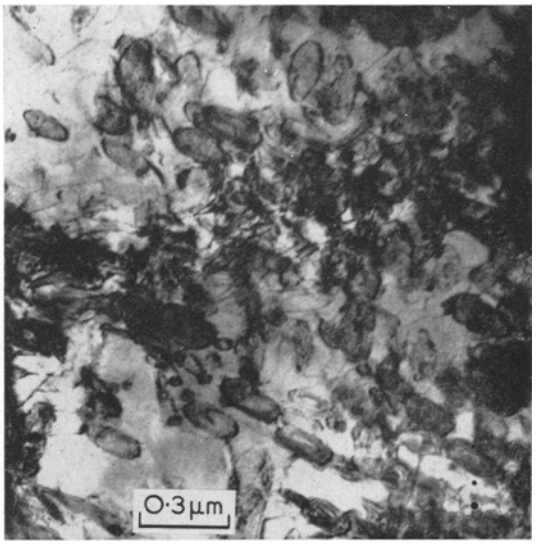

Figure 12 Rings of dislocation round small second phase particles after annealing 1 h at 550°C.

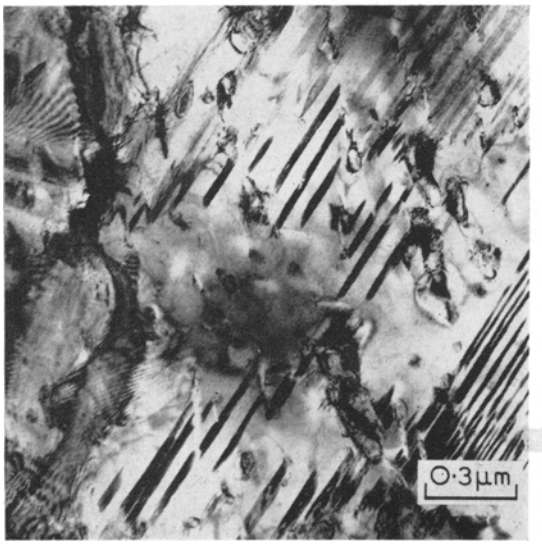

Figure 11 Narrow, parallel precipitates in a 1 h at 550°C specimen.

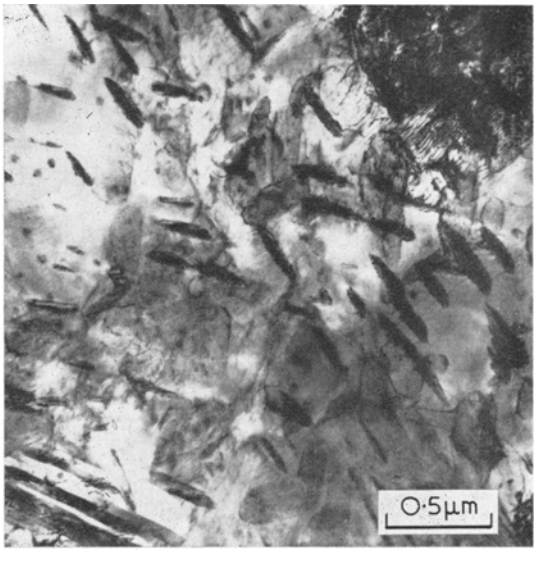

Figure 13 Characteristic microstructure after argon annealing at 550°C for 5 h.

mentioned above although some of the dislocations will doubtless result from local cross-slip of dislocations trying to avoid the precipitates.

A marked microstructural change results from annealing above 550°C. At 750°C, a rapid decrease in dislocation density through recovery occurs along with the appearance of large parallel precipitates of αTi-TiO. Like the 1 h at 550°C precipitates, these are believed formed by a martensitic shear process from supersaturated solid solution. Annealing times up to 5 h saw continued growth of these precipitates to a thickness of 100 to 500 nm (Figs. 14 and 15). The precipitates are generally seen to lie in a [4 3 1] direction while the twins, in Fig. 15, lie in [6 2 $\bar{1}$] and [3 4 3] directions, foil orientation [1 $\bar{2}$ 2] (directions and orientation with respect to the precipitate lattice). Occasionally, the precipitates were observed to consist of stacks of parallel plates, each platelet occurring at the intersection of two precipitates (Fig. 16). Such plates have been observed in a Ti-Mo alloy [84] and have been identified as thin twins. These are probably formed through the binary alloy crystal symmetry change, βTi cubic → αTi-TiO tetragonal, a reaction known to be invariably accompanied by an accumulation of sizeable strains [85] which can then be relieved by shear twinning of the order phase. Such behaviour has been observed in Cu-Au [86], Fe-Pt [87] and Ti-Mn [88].

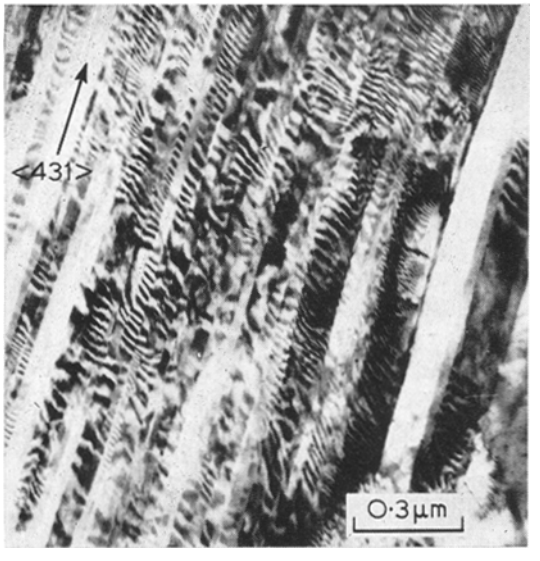

Figure 14 Fringe contrast effects on αTi-TiO precipitates in a 2 h at 750°C specimen, orientation (1$\bar{2}$2).

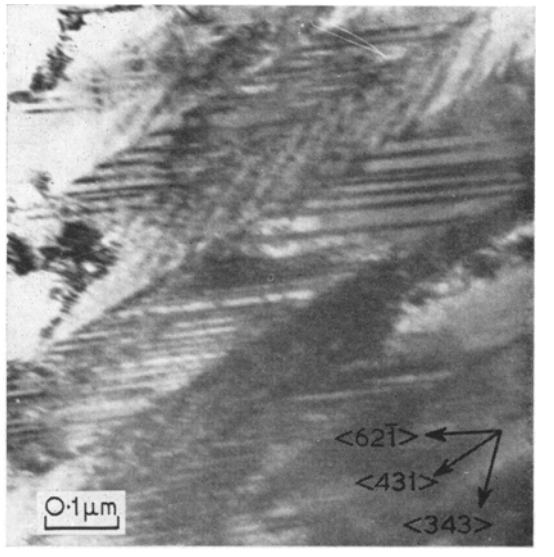

Figure 15 Large twinned αTi-TiO precipitates resulting from heating at 750°C for 5 h; orientation of foil (1$\bar{2}$2).

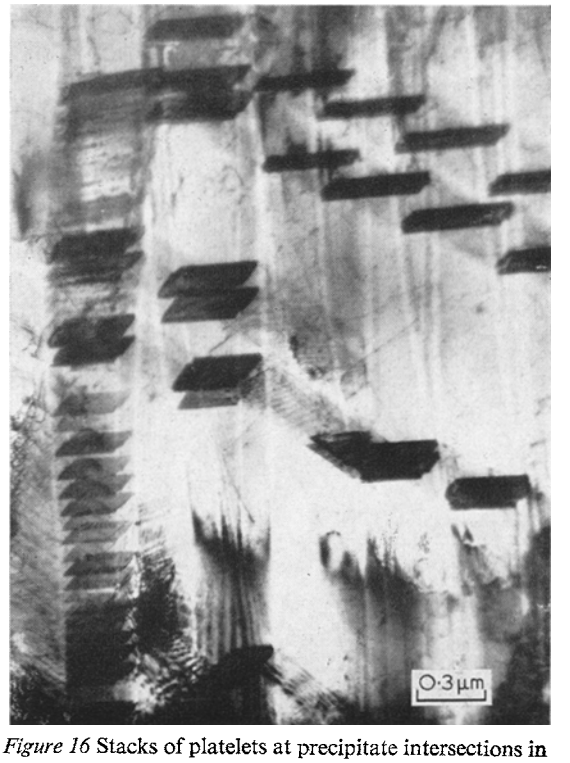

Figure 16 Stacks of platelets at precipitate intersections in 2 h at 750°C heated Nb-Ti.

5.4. Discussion of microstructure

Comparison between the precipitation sequence in vacuum- and argon-annealed material suggests that precipitates nucleated during argon-annealing can be expected to form a series of different oxides increasing in oxygen content with annealing time and temperature. Optical microscopy indicates that this is indeed the case. In contrast to vacuum-annealed specimens, optical micrographs of the surface of argon-annealed material show massive precipitates to be present. Surface precipitate nucleation occurred at about 400°C, the number of precipitates increasing with temperature of heat-treatment up to and including 550°C. The majority of these second-phase particles nucleated at the edge of the specimen and grew to the nearest edge, not by the shortest route, but in general in a straight line (Fig. 17). The precipitates were about 18 μm in width. Material heat-treated at 750°C showed relatively few of these precipitates, and those present did not traverse more than half the width of the specimen. The precipitates were indexed by X-ray diffraction as α-Ti or oxygen-enriched α-Ti. Bumps *et al* [82] have shown that the lattice parameters of α-Ti hardly change with oxygen addition and, hence, a more positive identification was not possible.

A similar massive precipitation effect has been reported by Hansen *et al* [89] in Ti-Mo and Ti-Nb alloys. These authors found that heating β-solid-solution samples in argon resulted in surface layer containing α phase stabilized by impurities, oxygen and/or nitrogen, while no contamination took place on heating in vacuum. Reference to the Ti-O phase diagram confirms that the extensive solubility of oxygen in α-Ti does cause an elevation in the $\alpha \rightleftharpoons \beta$ transformation temperature. In addition, the oxygen content of α-Ti can increase to about 33 at.% before a phase change occurs. For present results, however, this phase change is not realized for the surface precipitates since a change in impurity gradient through the specimen occurs at about 750°C.

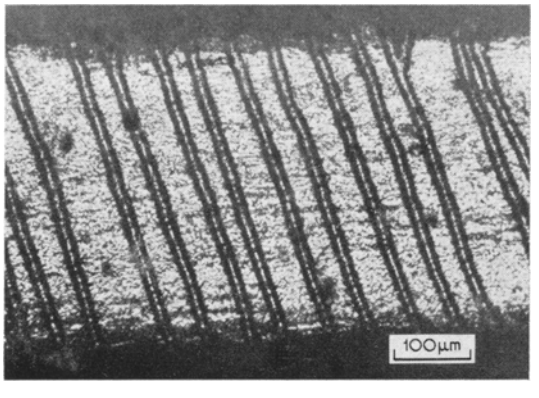

Figure 17 Optical micrograph of a 2 h at 550°C specimen showing parallel massive precipitates crossing the surface.

The whole precipitation process can be pictured to proceed as follows. In the vacuum-anneal case, although the vacuum is rather poor, most of the oxygen impurity can be considered to be already in solution before any heat-treatment occurs. A titanium sub-oxide, α-$TiO_{0.5}$, is initially precipitated throughout the material. This phase then increases in oxygen content and lattice parameter with increasing temperature of anneal. Only after prolonged heat-treatment at 550°C is αTi-TiO precipitated.

During the argon-anneal the same reaction occurs, complicated by the fact that the oxygen content of the alloy increases during the anneal owing to traces of oxygen in the argon. At low annealing temperatures, the oxygen diffusion time into the interior of the specimen is relatively long. An oxygen content gradient is developed through the Nb-Ti such that oxygen contamination is greatest at the surface of the specimen. Oxygen stabilization of α-Ti causes precipitation of the latter at the surface. Stabilization of α-Ti by oxygen has also been noted in bulk Nb-57Ti [76] and Nb-74Ti [90]. Higher annealing temperature and longer time causes further impurity absorption from the argon and hence the α-Ti precipitates increase in number; lattice parameter also increases with time and temperature up to about 750°C. While this process is occurring at the surface, the interior of the specimen is reacting in a similar but more complicated manner to that noted in the vacuum-annealed material. The addition of oxygen from the impure argon causes precipitates with a range of oxygen content, and induces the martensitic type of precipitation and associated twinning observed by Van Torne and Thomas [31] and others in Nb. More than one type of precipitate can occur at a given annealing temperature. At low annealing temperatures especially, the precipitates are probably non-equilibrium intermediate phases; hence the difficulty experienced in structure interpretation. A similar behaviour has been reported for some

Nb oxides [91]. In fact, the Nb-Ti phase diagram has not been published for temperatures below about 600°C since it appears that equilibrium would be almost impossible to achieve even after long-time annealings at these temperature levels [89].

At 750°C, oxygen diffusivity is about a factor of 10 greater than at 400°C [92]. Under these conditions, only a small amount of surface precipitation occurs before the impurity concentration gradient is removed and the whole specimen has become sufficiently impregnated with oxygen for bulk precipitation of the martensitic-like αTi-TiO phase.

The complexity of the precipitation process can be emphasized by reference to the Ti-O phase diagram [82, 93]. In a broad context, the βTi $\rightarrow$ (Ti, O) $\rightarrow$ series can be seen as an example of the familiar bcc/hcp/fcc transition, where the oxygen content acts as the controlling parameter. Similarly, the α-Ti/TiO equilibrium represents a transition from hexagonal to cubic close packing of metal atoms. In the latter case, successive oxygen occupation of octahedral holes in α-Ti should ideally result in an NiAs-type structure for TiO. This is found not to be the case, as occupation ceases when the anti-CdI_2-type structure of Ti_2O is reached and it transforms to the cubic symmetry of oxygen-deficient TiO [94]. The driving force behind the stacking change of the Ti atoms is the necessity for new oxygen sites. At high temperatures, this stacking change has been observed to occur via the intermediate stage of tetragonal Ti_3O_2. A process similar to the latter is believed to have occurred in the Nb-Ti alloy studied here. Unfortunately, since both the βTi-TiO series and the α-Ti/TiO equlibrium are relevant, the oxide transition modes are complicated. The final formation of the tetragonal phase αTi-TiO is not straightforward either since, although the high temperature form of TiO is indeed fcc, that at lower temperatures, such as 750°C, is tetragonal.

6. Normal state resistivity

The normal state resistivity, ρ_N, of material vacuum annealed at 550°C falls slowly with annealing (Fig. 18). This drop is associated with the annealing out of dislocations and the removal of oxygen from solid solution consequent upon the nucleation and growth of δ-TiO_x precipitates. Similar precipitation effects on ρ_N have been noted for Nb [95, 96]. The greater oxygen solubility of αTi-TiO compared to the lower oxides results in a still gradual decrease in matrix resistivity with longer annealing times. This effect has been reported for Nb-75Ti [90].

The effect of annealing in argon upon specimen resistivity is shown in Fig. 19. Heat-treatment at 400°C for 1 h results in an increase

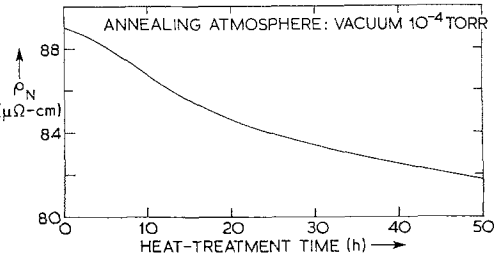

Figure 18 Specimen resistivity after annealing in vacuum of $1.33 \times 10^{-2} Nm^{-2}$ at 550°C, as a function of time.

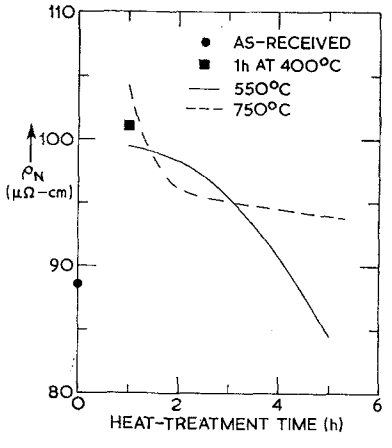

Figure 19 Specimen resistivity after annealing in argon at various temperatures, as a function of time.

of 14% in ρ_N. This is due to the migration of more dislocations to the cell boundaries; the arrangement of dislocations in a sufficiently fine cell-structure can give a higher resistivity than if uniformly distributed [97]. Annealing at 550°C causes ρ_N, after an initial rise, to drop, slowly at first, and then rapidly after longer times. The initial rise is partly due to dislocation rearrangement, and partly due to an increase in oxygen content. At longer times there is a balance between the addition of O_2 from the argon, and its removal along with titanium, from the matrix

by precipitation of the titanium sub-oxides. ρ_N of Nb-Ti alloys decreases with decreasing Ti content [98]. After several hours, precipitation is able to remove O_2 faster than it can be replaced by diffusion, resulting in the rapid drop in ρ_N. At higher temperatures the position is reversed, for example at 750°C the large initial increase in ρ_N decreases rapidly after short annealing times as precipitation takes place, but thereafter remains fairly constant as O_2 diffuses in at a rate equal to that which it is removed by precipitation.

7. Superconducting properties

The results of critical current measurements are shown in Figs. 20 and 21. Low field values are

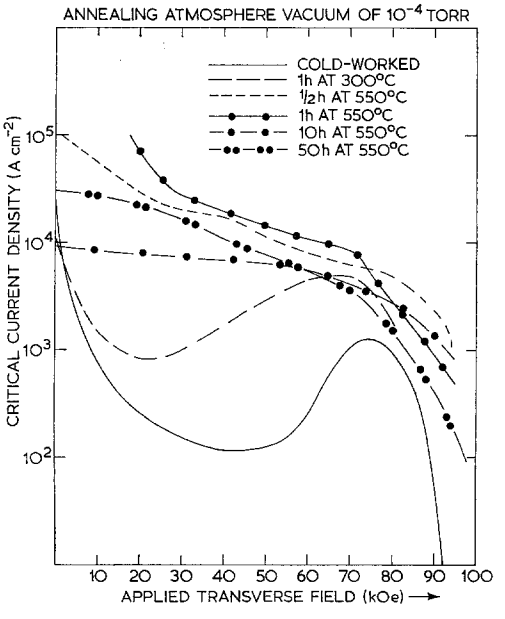

Figure 20 Critical current density at 4.2K versus applied magnetic field for vacuum annealed Nb-65 at. % Ti alloy.

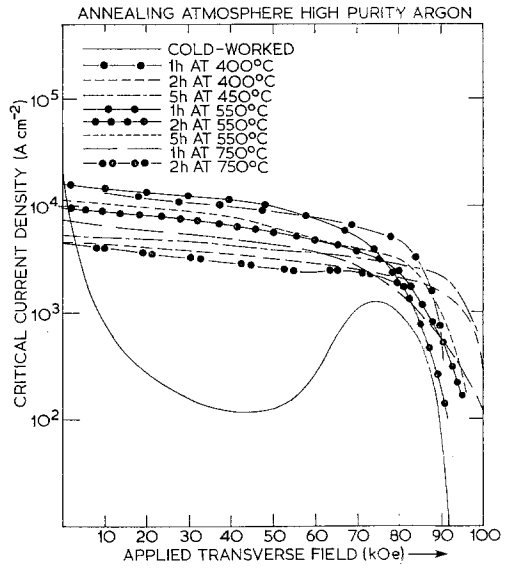

Figure 21 Critical current density at 4.2K versus applied magnetic field for argon annealed Nb-65 at. % Ti alloy.

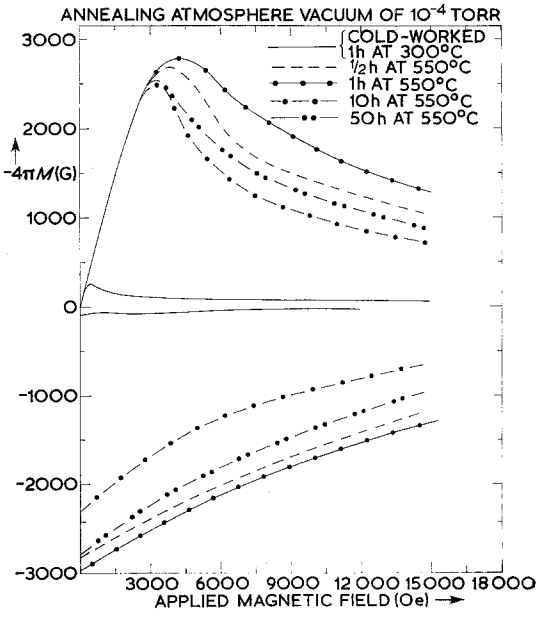

Figure 22 Low-field magnetization curves for specimens annealed in vacuum.

subject to error, as the normal phase may be nucleated at the current contracts, and lead to a pessimistic estimate of the critical current J_c. At higher fields the normal phase will be nucleated at the part of the specimen subjected to the highest field, which in these hairpin specimens is several centimetres from the current contacts. The high-field values of J_c may, therefore, be presumed to be reasonably accurate.

Measurements of specimen magnetization, shown in Figs. 22 and 23, are not subject to a contact problem, but with the laboratory facilities available could only be made at low fields. They are used here merely to check the accuracy of the low-field J_c results. The degree of hysteresis estimated from these curves places the specimens in the same relative order of merit

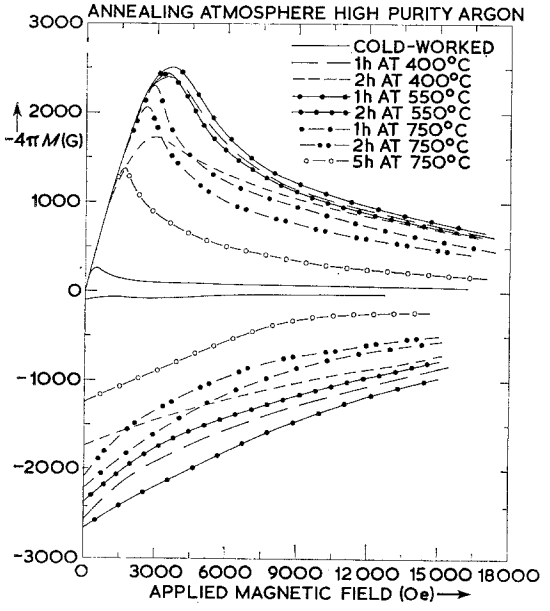

Figure 23 Low-field magnetization curves for specimens annealed in argon.

as that arrived at from the low-field J_c results. The conclusion is that the latter are accurate and that current contacts did not cause premature normality.

Flux-pinning behaviour is most conveniently represented by plotting the total Lorentz force $J_c \times B$, which, according to the critical state model [see ref. 1] is equal to the pinning force per unit volume, versus the reduced magnetic induction, b ($= B/B_{c2}$). The shape and position of the peak value(s) of this curve are characteristic of the particular mechanism of pinning; the peak height is a measure of the pinning strength. Here the results are plotted as $J_c \times H$ versus H; the difference between H and B for these specimens at fields $> H_{c1}$ is negligible. As H_{c2} could not be accurately determined it is not possible to use reduced units of H.

7.1. Upper critical field, H_{c2}

Though the actual values of upper critical field could not be determined, it is obvious from Figs. 20 and 21 that they were increased by annealing. H_{c2} would appear to increase with annealing time for specimens treated in vacuum, in contrast to the change in ρ_N. According to Berlincourt and Hake [99], the maximum in H_{c2} for the Nb-Ti system occurs at $\sim$ 60 at. % Ti. The slight reduction in Ti content of the matrix from 65 at. % as precipitation occurs may account for the increase in H_{c2}, though H_{c2} does not appear to vary much with composition over the range 60 to 65 at. % Ti. This explanation must also suffice for the argon-annealed specimens, as all show an increase in H_{c2} with annealing times, which corresponds to an ultimate fall in ρ_N, though the initial increase in ρ_N after very short anneals could account for the high estimated H_{c2} values for, for example, 1 h at 400°C and 1 h at 750°C specimens.

7.2. Flux-pinning in vacuum-annealed specimens

Curves of $J_c \times H$ ($\simeq$ Lorentz force) versus H for the vacuum annealed samples are plotted in Fig. 24. It is quite obvious that at least three

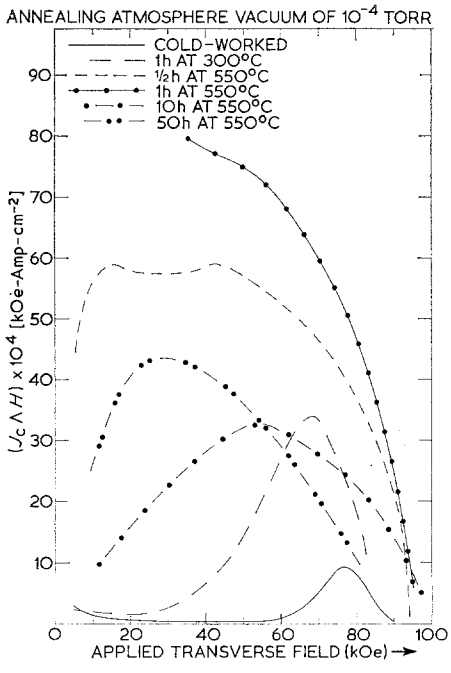

Figure 24 Lorentz force ($J_c \times H$) versus applied field, H, for Nb-Ti annealed in vacuum.

pinning mechanisms are operative. The untreated material shows a peak at $\sim$78 kOe, not far below H_{c2} ($\sim$90 kOe), with possibly a second peak at a very low field ($<$ 5 kOe). Pinning in this material is believed to be due solely to crystal dislocations, and these two peaks will be referred to as the dislocation (D) peaks. The specimen annealed for 10 h at 550°C shows a peak at 54 kOe ($\sim$0.5 H_{c2} for this

material), and after annealing for 50 h this is replaced by a peak at 28 kOe ($\sim 0.3\ H_{c_2}$). Precipitation is much in evidence in both of these specimens, and these peaks will be referred to respectively as the P and P′ peaks.

Annealing for 1 h at 300°C produces an increase in magnitude of the D peaks, with the high field peak shifted to the slightly lower field of 70 kOe. This is almost certainly due to the intrusion of a weak P peak. Half an hour at 550°C has increased the magnitude of both D peaks and the P peak; the latter now as high as the former. The trend continues for the 1-h anneal, and as with the previous specimen, it is difficult to distinguish the three separate peaks. Ten hours at 550°C results in an almost complete disappearance of the D peaks, leaving only the P; as mentioned above, lengthening the annealing time to 50 h replaces P by P′.

These results can be correlated with the microstructural changes reported in Section 5.2. The growth of the dislocation peaks in the early stages of annealing result from the increasing definition of the cell-structure as dislocations migrate from cells to cell walls, no doubt assisted by the diffusion of interstitials to the cell walls. Their subsequent disappearance is a direct consequence of the disintegration of the cell structure which is a precursor to recrystallization. The P peak is associated with the precipitation of $\delta TiO_{0.5}$, and P′ with its replacement by the α-Ti-TiO precipitates after longer annealing times. The actual pinning models associated with these microstructures are discussed later.

7.3. Flux-pinning in argon-annealed specimens

$J_c \times H$ versus H curves for the argon-annealed samples are shown in Fig. 25. In view of the much more complicated microstructures observed after annealing in argon, it is not surprising that the flux-pinning behaviour is also more complicated in these specimens, but it is possible to describe the curves as a mixture of the D and P peaks.

Annealing for 1 h at 400°C produces a peak at 65 kOe, which is $\sim 0.7\ H_{c_2}$ for this material. This would appear not to correspond to D, P or P′, but could, in fact, be made up of D and P peaks of almost equal magnitude. The annealing temperature for developing optimum dislocation pinning in a Nb-60 at. % Ti alloy is 385°C [58]. It can, therefore, be assumed that the 400°C

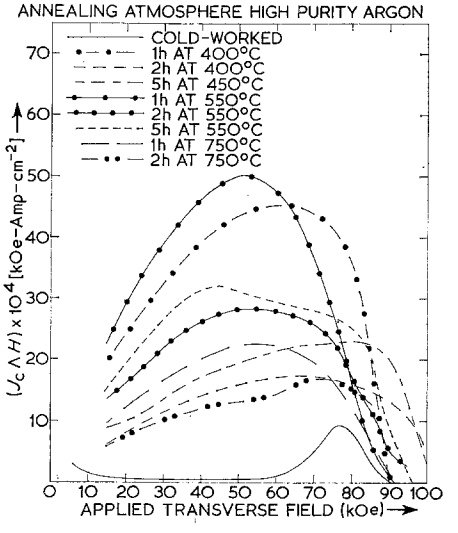

Figure 25 Lorentz force ($J_c \times H$) versus applied field, H, for Nb-Ti annealed in argon.

anneal produces near optimum dislocation pinning in this alloy, to which must be added the effect of the observed fine precipitation. Two hours at this temperature causes a considerable reduction in the height of this peak (or peaks) together with the largest observed increase in H_{c_2} to ~110 kOe. The 5 h at 450°C specimen shows what appears to be a reinforcement of the D peak. None of the low-temperature anneals succeeded in removing more than a portion of the original dislocation structure.

One hour at 550°C produces a large P peak, with little or no D content. Three types of precipitate morphology have been identified in this material; the pinning appears to be consistent with fine precipitates of the type shown in Fig. 11. Increasing the annealing time results in a lowering of this peak, and the appearance of a D peak. The latter could be associated with dislocations believed to be generated as a result of coherency strains.

Similar behaviour is observed after annealing at 750°C. The peak produced by the 1 h treatment is smaller than the 550°C peak, as might be expected from the larger size of the precipitates. Longer annealing times causes a reduction in the height of this peak, and a D peak now becomes evident. This may be due, not to dislocation pinning, but to a similar type of pinning by the twin boundaries within the large αTi-TiO precipitates.

No P′ peak was apparent in any of the argon-

annealed specimens. This peak, as will be discussed later, is believed to be associated with widely spaced, fairly coarse, precipitates; such precipitates were not seen in any of these specimens.

7.4. Pinning mechanisms

There is overwhelming evidence to show that strong flux-pinning is due to a microstructure which results in variation in superconducting properties with position [1]. The nature of the interaction between flux lines and the microstructure depends upon the scale of the latter with respect to the characteristic lengths of the superconductor [59]. When the size of the microstructural features (dislocation tangles, precipitates, etc.) and the distance between them is $\geqslant \lambda$, the super-conducting penetration depth, then flux can everywhere approach its equilibrium density [1, 97]. The interaction with flux lines is magnetic in origin, and the pinning force per unit volume [99] is

$$F_p(B) = \frac{S_v \, \Delta M(B) (\phi_0 B)^{\frac{1}{2}}}{1.07\lambda} \qquad (1)$$

where S_v is the surface area per unit volume of the pinning microstructure, $\Delta M(B)$ is the difference in equilibrium magnetization between matrix and pinning centre, and ϕ_0 is the flux quantum ($hc/2e = 2 \times 10^{-7}$G cm^{-2}).

When the pinning centres are non-superconducting precipitates $\Delta M(B)$ is equal to the reversible magnetization of the matrix; for $H > H_{c1}$ and $\kappa \gg 1$,

$$\Delta M(B) \simeq \frac{H_{c2} - H}{2.32\,\kappa^2}$$

and the Lorentz force is [1, 100]:

$$J_c \times B = \frac{\mu_0 S_v H_{c2}^2 h^{\frac{1}{2}}(1 - h)}{2.48\,\kappa^3} \cdot \qquad (2)$$

This function has a peak at $h(= H/H_{c2}) = 0.33$.

For pinning by a dislocation cell-structure [1, 97]:

$$\Delta M = \frac{(H_{c2} - 2H)\,\Delta\kappa}{2.32\,\kappa^3}$$

and the Lorentz force equation is:

$$J_c \times B = \frac{\mu_0 S_v H_{c2}^2 h^{\frac{1}{2}}(1 - 2h)\,\Delta\kappa}{2.48\,\kappa^4} \qquad (3)$$

where $\Delta\kappa$ is the difference in κ value between cell and cell-wall brought about by the increased resistivity of the latter. This function has peaks at $h = 0.17$ and at the upper critical field of the cells, which is less than the measured H_{c2} which will be that of the cell walls [97]. However, owing to non-uniformity of the microstructure, these peaks are broadened and appear at values of field below those given above [97].

If the variation in microstructure is on a scale finer than λ, then the flux density cannot vary with sufficient rapidity to conform to the value in local equilibrium with the microstructure. Pinning arises because of the variation in free energy of the flux line core across the microstructure. It has been suggested that, under these circumstances, pinning is associated with an elastic relaxation of the flux line lattice; the Lorentz force is given by an equation involving the elastic constants of the flux line lattice [101]. This sophisticated approach may not be necessary; at high current densities the flux lattice may be replaced by an "amorphous" state [102]. Hampshire and Taylor [59] find for very heavily cold-worked Nb-60 at. % Ti, with a dislocation cell-structure much finer than λ, that lattice elasticity can be ignored. Their relation for flux core pinning is:

$$J_c \times B = \frac{\mu_0 S_v H_{c2}^2 h(1 - h)\,\Delta\kappa}{2.67\,\kappa^3} \cdot \qquad (4)$$

This equation has a peak at $h = 0.5$. Although derived specifically for dislocation pinning, this expression is valid for pinning by any feature whose difference from the matrix can be described by a change in κ.

There are many other possible pinning mechanisms, and proposed expressions for the Lorentz force. The above have been chosen here because it is believed that Equations 2, 3 and 4 describe the experimentally observed behaviour identified in Sections 7.2 and 7.3 as the P′, D and P peaks respectively. It is now necessary to explain why it is thought that these are the appropriate mechanisms for heat-treated Nb-65 at. % Ti specimens.

7.5. Pinning and microstructure

The penetration depth for this alloy is $\sim$ 200 nm [59], and the cell diameter of the material prior to annealing is $\sim$ 300 nm. Dislocation pinning will, therefore, be via the magnetic interaction, and the Lorentz force will be described by Equation 3. The peak occurring just below H_{c2}, together with the sometimes observed peak at very low fields, in the unannealed or lightly-annealed specimens, can

readily be associated with this form of dislocation pinning. This peak appears to be present in specimens vacuum-annealed for 1 h at 300°C, ½ and 1 h at 550°C, and in material argon-annealed 1 and 2 h at 400°C, and 5 h at 450°C. In none of these specimens has the annealing treatment completely destroyed the original cold-worked dislocation cell-structure; in fact, short time low temperature anneals have enhanced the pinning characteristics of the structure. This is due to an increase in $\Delta\kappa$ brought about by a combination of dislocation migration from cell interiors to the cell walls as a precursor to polygonization, impurity diffusion to the cell-walls, and precipitation nucleated at the cell-walls. A dislocation peak also occurs in specimens annealed in argon for 5 h at 550°C and for 2 h at 750°C. In the former case, networks of dislocations are associated with precipitates, possibly generated as a result of coherency strain. The scale of these networks and the separation of groups of precipitates, at 200 to 400 nm, is sufficient to allow of magnetic pinning. No dislocations were observed in the 2 h at 750°C material. Precipitate size and separation, separation of faults at precipitate intersection, Fig. 16, and separation of twins within the precipitates, Fig. 15, are all $\gtrsim$ 200 nm, thus allowing the magnetic interaction to operate. Twin boundaries and stacking faults are expected to pin flux in a manner similar to that of dislocations [51].

The only heat-treatment which has apparently produced large, uniformly distributed precipitates of a definite second phase is that of a 50-h anneal at 550°C in vacuum. Significantly this is the only specimen which shows the P′ peak, whose position corresponds to the Lorentz force curve predicted by Equation 2. Pinning in this specimen should, therefore, be due to non-superconducting precipitates with a separation $\geqslant \lambda$. The former condition is met by the high oxygen content of the precipitates ($\simeq$ 40 at. %) and the latter as their spacing (200 to 1000 nm) is $\geqslant \lambda$ (200 nm).

All other heat-treated specimens show, to a greater or lesser extent, some evidence of the P peak at $h \simeq 0.5$. This is the behaviour described by Equation 4, and requires that pinning results from a change in κ of regions whose size and separation is $<\lambda$. It is likely that the features observed in the electron microscope are not true precipitates, but are regions enriched in titanium and oxygen. This change in composition could reduce κ without entirely destroying superconductivity in the "precipitates" and thus $\Delta\kappa$ pinning becomes appropriate. The spacing of these δ-TiO_x precipitates is extremely non-uniform; precipitates $\simeq$ 100 nm in width are distributed in clusters, the precipitate separation within the clusters is $\sim$ 100 nm, the separation between the clusters 500 to 1000 nm. This results from the nucleation of the precipitates on the original dislocation cell-structure, clusters of dislocations being formed in the most heavily dislocated regions. The flux-line core-energy interaction will give rise to interprecipitate pinning, and hence the P peak; weak inter-cluster pinning can occur via the magnetic interaction, making some contribution to the D peak.

Because of the non-uniformity of the observed microstructures, and because of a lack of knowledge of the superconducting properties of the precipitates, it is not possible to make quantitative comparisons between the observed values of the Lorentz force and the theoretical expressions given in Section 7.4. The above is self-consistent, and is regarded as the probable explanation of the experimental results.

8. Conclusions

The super-current density in niobium alloys containing interstitial impurities is increased by heat-treatment. In niobium-titanium alloys containing oxygen, existing theories of flux pinning can be invoked to correlate J_c with the precipitation of titanium oxides and sub-oxides. Considerations of stability require that superconductors should be produced as fine filaments in a normal metal matrix. The degree of deformation necessary to produce filaments cannot be achieved when interstitials are present in sufficient quantity to produce significant precipitation. Fortunately the very fine dislocation cell size resulting from high reductions gives flux-pinning and critical current densities comparable to those due to precipitation, and the latter is not recommended as a production route for commercial materials.

Acknowledgements

This work was financially supported by the Science Research Council. The authors are indebted to Professor E. R. Dobbs and the Physics Department at Lancaster for provision of facilities to pursue this work. They also wish to thank the Director of the Royal Radar Establishment, Malvern, for permission to use

the high field facilities. This paper is based in part on a thesis submitted for a Ph.D. degree at the University of Lancaster by M. J. Witcomb.

References

1. D. DEW-HUGHES, *Rep. Prog. Phys.* **34** (1971) 821.
2. A. V. NARLIKAR and D. DEW-HUGHES, *J. Mater. Sci.* **1** (1966) 317.
3. M. J. WITCOMB, A. ECHARRI, A. V. NARLIKAR, and D. DEW-HUGHES, *ibid* **3** (1968) 191.
4. W. CARRINGTON, K. F. HALE, and D. MCLEAN, *Proc. Roy. Soc.* **A259** (1960) 203.
5. A. S. KEH, "Direct Observations of Imperfections in Crystals" (Interscience, New York, 1962) p. 213.
6. A. S. KEH and S. WEISSMAN, "Electron Microscopy and Strength of Crystals" (Interscience, New York, 1963) p. 231.
7. R. BENSON, G. THOMAS, and J. WASHBURN, "Direct Observations of Imperfections in Crystals" (Interscience, New York, 1962) p. 375.
8. J. O. STIEGLER, C. K. H. DUBOSE, R. E. REED, and C. J. MCHARGUE, *Acta Metallurgica* **11** (1963) 851.
9. A. V. NARLIKAR, Ph.D. thesis, University of Cambridge (1965).
10. W. S. OWEN, A. GILBERT, C. N. REID, D. HULL, and I. MATROR, see C. S. BARRETT, "The Cold Working of Metals" (Amer. Soc. Metals, Cleveland, Ohio, 1949) p. 65.
11. D. HULL, I. D. MCIVOR, and W. S. OWEN, "The Relation between the Structure and Mechanical Properties of Metals" (London, H.M.S.O., 1963) p. 596.
12. F. O. JONES, "Niobium, Tantalum, Molybdenum and Tungsten" (Elsevier, Amsterdam, 1961) p. 158.
13. Y. NAKAYAMA, S. WEISSMAN, and T. IMURA, "Direct Observations of Imperfections in Crystals" (Interscience, New York, 1962) p. 573.
14. A. V. NARLIKAR, unpublished work.
15. R. E. SMALLMAN, "Modern Physical Metallurgy" (Butterworths, London, 1970) p. 391.
16. A. HOWIE, "Direct Observations of Imperfections in Crystals" (Interscience, New York, 1962) p. 283.
17. M. J. WITCOMB, to be published.
18. R. W. K. HONEYCOMBE, "The Plastic Deformation of Metals" (Edward Arnold, London, 1968) p. 267.
19. *Idem, ibid* p. 306.
20. A. H. COTTRELL, "Report on Strength of Solids" (Phys. Soc., London, 1948) p. 30.
21. D. MCLEAN, "Mechanical Properties of Metals" (Wiley, New York, 1962) p. 189.
22. R. H. DOREMUS and E. F. KOCH, *Trans. AIME* **218** (1960) 591.
23. A. S. KEH and H. A. WRIEDT, *ibid* **224** (1962) 560.
24. C. DOLLINS and C. WERT, *Acta Metallurgica* **17** (1969) 711.
25. J. P. CHARLESWORTH and P. E. MADSEN, Atomic Energy Research Establishment, Harwell, Report no. AERE-R6534, (1970) p. 26.
26. Ref. 15, p. 160.
27. R. W. CAHN, "Physical Metallurgy" (North Holland, Amsterdam, 1965) p. 207.
28. J. VAN LANDUYT, *Quart. Rep.* **3** (1963) 5.
29. *Idem, Phys. Stat. Sol.* **6** (1964) 957.
30. J. VAN LANDUYT, R. GEVERS, and S. AMELINCKX, *ibid* **13** (1966) 467.
31. L. I. VAN TORNE and G. THOMAS, *Acta Metallurgica* **12** (1964) 601.
32. R. E. VILLAGRANA and G. THOMAS, *Phys. Stat. Sol.* **9** (1965) 499.
33. D. HULL and D. C. WYNNE, Proceedings of the 3rd European Regional Conference on Electron Microscopy, Prague, 1964 (Czech. Acad. Sci., Prague, 1965) p. 239.
34. D. P. SERAPHIM, N. R. STEMPLE, and D. T. NOVICK, *J. Appl. Phys.* **33** (1962) 136.
35. J. L. SNOEK, *Physica* **8** (1941) 711.
36. G. SCHOECK and A. SEEGER, *Acta Metallurgica* **7** (1958) 469.
37. C. S. BARRETT and T. B. MASSALSKI, "Structure of metals" (McGraw-Hill, New York, 1966) p. 486.
38. H. J. GOLDSCHMIDT, "Interstitial Alloys" (Butterworths, London, 1967) p. 48.
39. A. R. G. BROWN, D. CLARKE, J. EASTERBROOKE, and K. S. JEPSON, *Nature* 201 (1964) 914.
40. B. A. HATT and V. G. RIVLIN, *J. Phys. D.* **1** (1968) 1145.
41. L. BAKER and J. SUTTON, *Phil. Mag.* **19** (1969) 1223.
42. A. T. BALCERZAK and S. L. SASS, *Trans. Met. Soc. AIME* **3** (1972) 1601.
43. L. A. BAGARIATSKII, G. L. NOSOVA, and T. V. TAGUNOVA, *Sov. Phys. Doklady* (trans) **3** (1959) 1014.
44. M. OKA, C. S. LEE, and K. SHIMIZU, *Trans. Met. Soc. AIME* **3** (1972) 37.
45. B. A. ROGERS and D. F. ATKINS, *ibid* **7** (1955) 1034.
46. E. M. SAVITSKII, M. A. TYLKINA, and I. A. TSYGENOVA, *Zh. Neorg. Khim.* **9** (1969) 1960.
47. YU. V. EFIMOV, V. V. BARON, and E. M. SAVITSKII, "Physics and Metallography of Superconductors", ed. E. M. Savitskii and V. V. Baron (Consultants Bureau, New York, 1970) p. 69.
48. C. W. BERGHOUT, *Phys. Letters* **1** (1962) 292.
49. G. W. J. WALDRON, *J. Less Common Metals* **17** (1969) 167.
50. J. D. LIVINGSTONE and H. W. SCHADLER, *Prog. Mater. Sci.* **12** (1964) 183.
51. G. J. VAN GURP, and D. J. VAN OOIJEN, *J. Physique* **27** (1966) C3.
52. D. DEW-HUGHES, *Mater. Sci. Eng.* **1** (1966) 2.
53. M. J. WITCOMB, and A. V. NARLIKAR, *Phys. Stat. Sol. (a)* **11** (1972) 311.
54. M. S. WALKER, R. STICKLER, and F. E. WERNER, "Metallurgy of Advanced Electronic Materials", ed. G. E. Brock (Interscience, New York, 1962) p. 49.
55. I. MILNE, *J. Mater. Sci.* **7** (1972) 413.
56. J. P. CHARLESWORTH and P. E. MADSEN, Atomic Energy Research Establishment, Harwell, report

nos. AERE-R6634 (1970), AERE-R6729 (1971), AERE-R6779 (1971).
57. C. BAKER, *J. Mater. Sci.* **5** (1970) 40.
58. D. F. NEAL, A. C. BARBER, A. WOOLCOCK, and J. A. F. GIDLEY, *Acta Metallurgica* **19** (1971) 143.
59. R. G. HAMPSHIRE and M. T. TAYLOR, *J. Phys. F. Metal Physics* **2** (1972) 89.
60. R. R. HAKE, D. H. LESLIE, and T. G. BERLINCOURT, *Phys. Rev.* **127** (1962) 170.
61. R. R. HAKE, T. G. BERLINCOURT, and D. H. LESLIE, *Bull. Amer. Phys. Soc.* **6** (1961) 425.
62. *Idem*, Proc. AIME Symp. Superconducting Materials 1962 (Interscience, New York).
63. R. R. HAKE, D. H. LESLIE, and C. G. RHODES, Proc. 7th Int. Conf. on Low Temperature Physics (Butterworths, London, 1963) p. 342.
64. C. BAKER and M. T. TAYLOR, *Phil Mag.* **16** (1967) 1129.
65. T. G. BERLINCOURT, R. R. HAKE, and D. H. LESLIE, *Phys. Rev. Letters* **6** (1961) 671.
66. J. J. HAUSER and R. G. TREUTING, *J. Phys. Chem. Solids* **24** (1963) 371.
67. I. PFEIFFER and H. HILLMAN, *Acta Metallurgica* **16** (1968) 1429.
68. T. DOI, F. ISHIDA, U. KAWABE, and M. KITADA, *Trans. Met. Soc. AIME* **242** (1968) 1793.
69. T. DOI, F. ISHIDA, and U. KAWABE, *J. Appl. Phys.* **38** (1967) 3811.
70. J. SUTTON and C. BAKER, *Phys. Letters* **21** (1966) 601.
71. D. KRAMER and C. G. RHODES, *Trans. Met. Soc. AIME* **239** (1967) 1613.
72. J. PENNEY, W. D. HOFF, and W. J. KITCHINGHAM, *J. Phys. D; Applied Physics* **3** (1970) 125.
73. J. D. BETTERTON, G. D. KNEIP, D. S. EASTON, and J. O. SCARBOROUGH, "Superconductors" (Interscience, New York, 1962) p. 61.
74. G. W. J. WALDRON, *J. Mater. Sci.* **4** (1969) 290.
75. Y. N. KUNAKOV, E. V. KACHUR, and V. Y. PAKHOMOV, ref. 47, p. 64.
76. F. W. REUTER, K. M. RALLS, and J. WULFF, *Trans. Met. Soc. AIME* **236** (1966) 1143.
77. G. C. RAUCH, T. H. COURTNEY, and J. WULFF, *ibid* **242** (1968) 2263.
78. R. GEVERS, P. DELAVIGNETTE, H. BLANK, J. VAN LANDUYT, and S. AMELINCKX, *Phys. Stat. Sol.* **5** (1964) 595.
79. D. J. VAN OOIJEN and A. S. VAN DER GOOT, *Philips Res. Report* **20** (1965) 162.
80. D. A. WARD, *Cryogenics* **7** (1967) 41.
81. S. ANDERSON, *Acta Chem. Scand.* **13** (1959) 415.
82. K. S. BUMPS, H. D. KESSLER, and M. HANSEN, *Trans. Amer. Soc. Metals* **45** (1953) 1008.
83. R. B. NICHOLSON, G. THOMAS, and J. NUTTING, *J. Inst. Metals* **87** (1958-9) 429.
84. M. J. BLACKBURN and J. C. WILLIAMS, *Trans. Met. Soc. AIME* **239** (1967) 287.
85. L. E. TANNER and M. F. ASHBY, *Phys. Stat. Sol.* **33** (1969) 59.
86. B. HANSEN and R. S. BARNES, *Acta Metallurgica* **12** (1964) 315.
87. H. LIPSON, D. SCHOENBERG, and G. V. STUPART, *J. Inst. Metals* **67** (1941) 333.
88. C. HAMMOND and P. M. KELLY, *Acta Metallurgica* **17** (1969) 869.
89. M. HANSEN, E. L. KAMEN, H. D. KESSLER, and D. J. MCPHERSON, *Trans. Met. Soc. AIME* **191** (1951) 881.
90. R. L. RICKETTS, T. H. COURTENAY, L. A. SHEPARD, and J. WULFF, *Trans. Met. Soc. AIME* **1** (1970) 1537.
91. K. A. JONES and R. M. ROSE, *Trans. Met. Soc. AIME* **245** (1969) 67.
92. A. D. MCQUILLAN and M. K. MCQUILLAN, "Titanium" (Butterworths, London, 1956).
93. P. EHRLICH, *Z. Elektrochem* **45** (1939) 90.
94. H. J. GOLDSCHMIDT, "Interstitial Alloys" (Butterworths, London, 1967) p. 377.
95. C. Y. ANG and C. WERT, *Trans. AIME* **197** (1953) 1032.
96. W. DE SORBO, *Phys. Rev.* **132** (1963) 107.
97. D. DEW-HUGHES and M. J. WITCOMB, *Phil. Mag.* **26** (1972) 73.
98. T. G. BERLINCOURT and R. R. HAKE, *Phys. Rev.* **131** (1963) 140.
99. A. M. CAMPBELL, J. E. EVETTS, and D. DEW-HUGHES, *Phil. Mag.* **18** (1968) 313.
100. R. I. COOTE, J. E. EVETTS, and A. M. CAMPBELL, *Canad. J. Phys.* **50** (1972) 421.
101. W. A. FIETZ and W. W. WEBB, *Phys. Rev.* **178** (1969) 657.
102. H. TRAUBLE and U. ESSMANN, *J. App. Phys.* **39** (1968) 4052.

Received 12 February and accepted 28 February, 1973.